

# Analytical results for the superflow of spin-orbit-coupled Bose-Einstein condensates in optical lattices

Xiaobing Luo<sup>1,2,3,\*</sup>, Zhou Hu<sup>1</sup>, Zhao-Yun Zeng<sup>2</sup>, Yunrong Luo<sup>4</sup>, Baiyuan Yang<sup>2</sup>, Jinpeng Xiao<sup>2</sup>, Lei Li<sup>2</sup>, and Ai-Xi Chen<sup>1</sup>

<sup>1</sup>*Department of Physics, Zhejiang Sci-Tech University, Hangzhou, 310018, China*

<sup>2</sup>*School of Mathematics and Physics, Jingtangshan University, Ji'an 343009, China*

<sup>3</sup>*State Key Laboratory of Low-Dimensional Quantum Physics,*

*Department of Physics, Tsinghua University, Beijing 100084, China and*

<sup>4</sup>*Department of Physics and Key Laboratory for Matter Microstructure and Function of Hunan Province, and Key Laboratory of Low-dimensional Quantum Structures and Quantum Control of Ministry of Education, Hunan Normal University, Changsha 410081, China*

(Dated: August 30, 2022)

In this paper, we show that for sufficiently strong atomic interactions, there exist analytical solutions of current-carrying nonlinear Bloch states at the Brillouin zone edge to the model of spin-orbit-coupled Bose-Einstein condensates (BECs) with symmetric spin interaction loaded into optical lattices. These simple but generic exact solutions provide an analytical demonstration of some intriguing properties which have neither an analog in the regular BEC lattice systems nor in the uniform spin-orbit-coupled BEC systems. It is an analytical example for understanding the superfluid and other related properties of the spin-orbit-coupled BEC lattice systems.

PACS numbers:

## I. INTRODUCTION

As an intrinsic interaction between the motion and spin of a particle, spin-orbit (SO) coupling in solid-state materials plays an important role in many interesting physical phenomena and applications, such as topological insulators[1], spin Hall effect[2], and spin devices[3], etc. Recently, artificial SO-coupling has been successfully realized in both bosonic and fermionic ultracold atomic systems[4]-[9], which provides a brand new platform to explore these exotic states and SO-coupled superfluids. The SO-coupled atomic systems exhibit many novel phases that have no parallel in conventional condensed matter physics. For a Bose-Einstein condensate (BEC) in homogeneous space, the experimentally accessible spin-orbit coupling gives rise to a class of nontrivial superfluid phase[10]-[12] and collective excitations[13, 14]. For example, the ground-state phase diagram for a homogeneous spin-orbit-coupled BEC is demonstrated to include a stripe phase with periodic density modulation that breaks continuous translation symmetry[10, 11, 15].

SO-coupled BECs in optical lattices have also received considerable attentions[16]-[21], due to the rich emergent physics stemming from the interplay between SO coupling and lattice effects. In a recent experiment, SO-coupled BECs in an optical lattice have been successfully loaded into the destined nonlinear Bloch band, and the dynamical stabilities of Bloch states crucial to the superfluidity of a BEC have been measured[22], which provides a direct observation of the broken Galilean invariance. On the theoretical side, the flat band dispersion of such SO-coupled lattice systems has been uncovered[20] and a full ground state phase diagram in the superfluid regime has been analyzed by numerical studies[23].

For the fundamental importance it is extremely valuable to have analytic solutions to the theoretical model of BECs in optical lattices, in that they can provide a deeper understanding of the underlying physics than straight numerical simulations. The research activities of finding exact analytic solutions to regular BECs in periodic potentials have been under way for a long time and a large family of exact stationary solutions have been derived. Several known models that have exact analytical solutions include the one-component BEC in quasi-one-dimensional Kronig-Penney potential[25, 36], and quasi-one-dimensional (or two-dimensional) Jacobi elliptic potential (which can be reduced to a sinusoidal potential in the limit case)[26]-[29]. These analytic results have been generalized to multi-component (including two-component) regular BECs without SO coupling[30, 31]. Due to the advantage of being analytically tractable, these accurate solutions can serve as good examples for understanding the appearance of loops (swallowtails) in the Bloch band structure which are related to superfluid properties of the BEC[32]-[40]. For example, Wu and Niu have used a simple exact nonlinear Bloch solution (which connects the loop to the rest of the Bloch band) to illustrate the multiple-valuedness of lowest band at the Brillouin zone edge which makes it different from the linear Bloch band[32, 41].

Interestingly, such a looplike dispersion relation has also been found recently in a SO-coupled BEC in free space[42]. However, the presence of SO coupling poses a challenge to finding the exact solutions to the BEC systems with periodic potentials and the corresponding exact solutions to such systems remain extremely rare. Recently, a type of spatiotemporal Bloch state of two-component SO-coupled BEC in a high-frequency driven optical lattice has been obtained analytically, which nevertheless needs fine tuning of the system parameters to match the rigorous equilibrium condition and therefore has no generic nature[43]. Thus, it is highly desirable and worthwhile to seek for generic exact solutions to the systems of SO-

---

\*Corresponding author: xiaobingluo2013@aliyun.com

coupled BECs in optical lattices, which will certainly help to better understand the superfluid and other physical properties of SO-coupled lattice BEC systems.

In this paper, we present a set of analytical degenerate Bloch wave solutions for SO-coupled BEC in an optical lattice. These analytic solutions exist only for sufficiently large interaction strength and connect to a known solution in the limit of zero SO coupling. Their properties related to superfluidity are fully analyzed. It is analytically demonstrated that SO coupling adds some results to the superfluidity of condensates at the Brillouin zone edge. For example, these exact nonlinear Bloch wave states can carry a pure spin current and no total atomic density current. They also provide an analytical evidence for the looplike Bloch band structure in the SO-coupled BEC lattice system. By using the standard Bogoliubov theory, these exact solutions are examined and shown to have both Landau and dynamical stabilities in certain parameter regions.

## II. MODEL EQUATION

We consider the mean-field model of a quasi-one-dimensional SO-coupled BEC in the presence of an optical lattice along  $x$  direction given by a periodic potential  $V(x) = V_0 \sin^2(k_L x)$ , where  $k_L = 2\pi/\lambda_L$  is the wavenumber of the laser beam with  $\lambda_L$  being the laser wavelength, and  $V_0$  is the lattice depth. The dynamics of such a SO-coupled BEC system can be described by the dimensionless Gross-Pitaevskii (GP) equation,

$$i\frac{\partial\Psi}{\partial t} = [\hat{H}_{\text{soc}} + V_0 \sin^2(x) + \hat{H}_{\text{non}}]\Psi, \quad (1)$$

where  $\Psi = (\Psi_1, \Psi_2)^T$  is the spinor describing the two pseudospin components of the BEC,  $\hat{H}_{\text{soc}}$  is the single-particle SO-coupled Hamiltonian,

$$\hat{H}_{\text{soc}} = \frac{\hat{p}_x^2}{2} + k_0 \hat{p}_x \hat{\sigma}_z + \frac{\Omega}{2} \hat{\sigma}_x, \quad (2)$$

and the nonlinear terms originating from the atomic interactions are explicitly given by

$$\hat{H}_{\text{non}} = \begin{pmatrix} g_{11} |\Psi_1|^2 + g_{12} |\Psi_2|^2 & 0 \\ 0 & g_{22} |\Psi_2|^2 + g_{12} |\Psi_1|^2 \end{pmatrix}. \quad (3)$$

The model (1) has been realized in the very recent experiment by Hamner *et al*[22]. In the above dimensionless GP equation,  $\hat{p}_x = -i\partial_x$  is the atomic momentum operator,  $\hat{\sigma}_{x,y,z}$  are the usual  $2 \times 2$  Pauli matrices,  $\Omega$  is the Raman frequency, and  $k_0 = k_R/k_L$  characterizes the SO coupling strength which is determined by the wave number of the Raman laser  $k_R$ . The units of energy, time, and length are chosen as  $2E_L = \hbar^2 k_L^2/m$  with  $m$  being the atomic mass,  $m/(\hbar k_L^2)$ , and  $1/k_L$ , respectively. The effective one-dimensional atomic interactions are given by  $g_{ij} = \hbar\omega_\perp n_0 a_{ij}/E_L$  ( $i, j = 1, 2$ ), where  $a_{ij}$  is the s-wave scattering length of spin components  $i$  and  $j$ ,  $\omega_\perp$  is the transversal trapping frequency, and  $n_0 = N/L_x$  is the averaged BEC density with  $N$  being the atom number in one

unit cell and  $L_x = \lambda_L/2 = \pi/k_L$  the period of the optical lattice. In the present work, we consider the condensate in a cigar-type trapped potential with the transversal frequency  $\omega_\perp$  much larger than the longitudinal one. The two-component wavefunction  $\Psi(x)$  is normalized in units of  $\sqrt{n_0}$ , such that the normalization condition turns out to be

$$\frac{1}{\pi} \int_{-\pi/2}^{\pi/2} dx (|\Psi_1|^2 + |\Psi_2|^2) = 1. \quad (4)$$

The dimensionless GP system (1) can also be viewed as a Hamiltonian system governed by the grand canonical Hamiltonian

$$H = \frac{1}{\pi} \int_{-\pi/2}^{\pi/2} dx \left\{ \Psi^\dagger [\hat{H}_{\text{soc}} + V_0 \sin^2(x)] \Psi + \frac{g_{11}}{2} |\Psi_1|^4 + \frac{g_{22}}{2} |\Psi_2|^4 + g_{12} |\Psi_1|^2 |\Psi_2|^2 - \mu |\Psi|^2 \right\}, \quad (5)$$

where  $\mu$  is the chemical potential. Among all possible solutions of equation (1), there are states which still have the form of Bloch waves, i.e.,  $\Psi(x, t) = \psi(x) \exp(-i\mu t) = \varphi_k(x) \exp(ikx - i\mu t)$ , where  $\varphi_k(x)$  is a periodic function of period  $\pi$  and  $k$  is the Bloch wave number. The solutions  $\psi(x) = (\psi_1(x), \psi_2(x))^T$  can be found by extremizing the Hamiltonian (5) and satisfy the stationary GP equation,

$$[\hat{H}_{\text{soc}} + V_0 \sin^2(x) + g(|\psi_1|^2 + |\psi_2|^2)]\psi = \mu\psi. \quad (6)$$

For simplicity, in Eq. (6), we have assumed a SU(2)-symmetric spin interaction with all equal nonlinearities  $g_{11} = g_{22} = g_{12} = g$  unless explicitly stated otherwise. This assumption is reasonable because the regime where the nonlinear coefficients are fully tunable for SO-coupled BECs can be achieved in the experiment[44].

## III. EXACT NONLINEAR BLOCH WAVES

In the previous work[23], the ground-state phase diagram of the SO-coupled lattice system (1) has been numerically studied, and an unexpected result is that a single momentum phase (a Bloch wave) with zero longitudinal ( $\langle\sigma_z\rangle$ ) and nonzero transverse ( $\langle\sigma_x\rangle$ ) spin polarization appears at the Brillouin zone edge, which has no counterpart in the uniform system. Generally, it is hard to find exact analytical solutions for such a complex nonlinear system. However, here we will show that for sufficiently strong SU(2)-symmetric spin interactions, there exists a family of generic exact analytical Bloch solutions to the GP equation (1) for a condensate with a wave vector  $k = \pm 1$  corresponding to the boundary of the first Brillouin zone. Using the trial solution method (see details in Appendix), we obtain the exact Bloch solution of Eq. (6) as follows:

$$\begin{pmatrix} \psi_1 \\ \psi_2 \end{pmatrix} = C_1 \begin{pmatrix} \sin \frac{\theta}{2} \\ -\cos \frac{\theta}{2} \end{pmatrix} e^{ix} + C_2 \begin{pmatrix} \cos \frac{\theta}{2} \\ -\sin \frac{\theta}{2} \end{pmatrix} e^{-ix}, \quad (7)$$

$$C_{1,2} = \frac{\sqrt{g + \frac{V_0}{2\sin\theta}} \pm \sqrt{g - \frac{V_0}{2\sin\theta}}}{2\sqrt{g}},$$

with

$$\sin \theta = \frac{\Omega}{2\sqrt{\frac{\Omega^2}{4} + k_0^2}}, \quad \cos \theta = \frac{k_0}{\sqrt{\frac{\Omega^2}{4} + k_0^2}}. \quad (8)$$

In Eq. (7), the plus in the plus/minus ( $\pm$ ) sign is for  $C_1$ , and the minus is for  $C_2$ . We can easily prove this exact solution by directly substituting Eqs. (7) and (8) into the stationary GP equation (6). Upon this substitution, we have  $\mu = 1/2 + g + V_0/2 - \sqrt{\Omega^2/4 + k_0^2}$ . This solution is a nonlinear Bloch wave state at the edge of the Brillouin zone, which only exists when the all-equal nonlinear coefficient is above a critical value, i.e.,  $\tilde{g} = 2g \sin \theta / V_0 \geq 1$ . Apparently, the extra nonlinear Bloch wave state has no counterpart in the linear case.

When  $k_0 = 0$  (in the absence of SO coupling), we have  $\sin \theta = 1$  and the exact solution (7) can be reduced to the solution discovered previously in the regular BEC [26]

$$\psi_1 = -\psi_2 = \sqrt{-\frac{V_0}{2g} \sin^2(x) + \frac{B}{2g}} \exp[i\Theta(x)], \quad (9)$$

where

$$\begin{aligned} \tan[\Theta(x)] &= \sqrt{1 - V_0/B} \tan(x), \\ B &= g + V_0/2, \end{aligned} \quad (10)$$

with the chemical potential  $\mu = B + 1/2 - \Omega/2$ . Note that the notations of Hamiltonian used here differ slightly from the ones in Ref. [26]. If we make the following substitutions:  $g_{11} + g_{22} = 2g = 1, \Omega = 0, V_0 \rightarrow -V_0$ , Eq. (9) exactly recovers the one [Eq. (10) of Ref. [26], the solution connecting the famous loop with the rest of the Bloch band] discovered previously in the regular BEC (without SO coupling) lattice systems.

For a more intuitive description of the existence condition of the exact solution, in Fig. 1 we have plotted the critical lines satisfying  $\tilde{g} = 1$  for the different parameter sets. It is clearly seen that the critical values of  $g$  monotonically increase with the SO coupling strength  $k_0$  for any fixed Rabi frequency  $\Omega$ , and increasing Rabi frequency  $\Omega$  will lower the critical values of  $g$  for the exact solution to exist. The minimum critical value of  $g/V_0 = 1/2$  exists at  $k_0 = 0$ .

Performing the complex conjugation of Eq. (6) and then comparing it with its original equation, we conclude that for any solution  $(\psi_1, \psi_2)^T$  given by Eqs. (7) and (8),  $(e^{i\delta}\psi_2^*, e^{i\delta}\psi_1^*)^T$  is also a solution of Eq. (6) with the same chemical potential for arbitrary global phase  $\delta$ . Without loss of generality, we choose  $\delta = \pi$  and use notations of Eqs. (7)-(8) to express the other exact solution in the simple form

$$\begin{aligned} \begin{pmatrix} \psi_1 \\ \psi_2 \end{pmatrix} &= C_1 \begin{pmatrix} \sin \frac{\theta}{2} \\ -\cos \frac{\theta}{2} \end{pmatrix} e^{ix} + C_2 \begin{pmatrix} \cos \frac{\theta}{2} \\ -\sin \frac{\theta}{2} \end{pmatrix} e^{-ix}, \\ C_{1,2} &= \frac{\sqrt{g + \frac{V_0}{2\sin\theta}} \mp \sqrt{g - \frac{V_0}{2\sin\theta}}}{2\sqrt{g}}. \end{aligned} \quad (11)$$

The solutions (7) and (11) would show explicitly the symmetry by interchange of  $C_1$  and  $C_2$ . That is to say, the solution

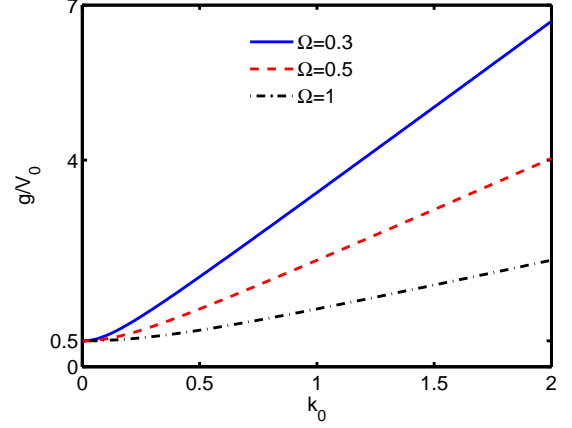


FIG. 1: (color online) The critical values of  $g/V_0$  versus the SO coupling strength  $k_0$  for different Rabi frequencies  $\Omega = 0.3, \Omega = 0.5$  and  $\Omega = 1$ . The critical lines are given by  $\tilde{g} = 2g \sin \theta / V_0 = 1$ , above which the exact solution (7) exists for the stationary GP equation (6). Plotted quantities are in normalized units.

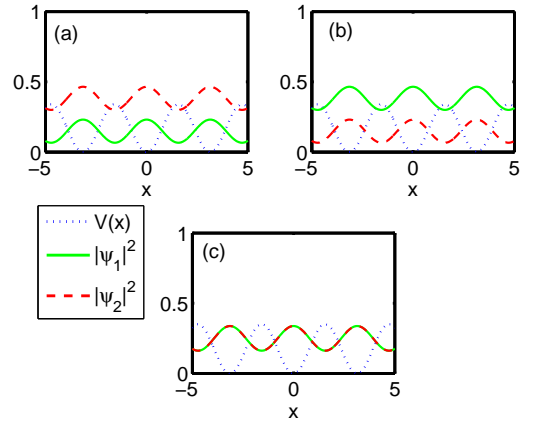


FIG. 2: (color online) Density profiles along the  $x$  direction and the corresponding potential functions. (a)-(b):  $V_0 = 0.34$  satisfying  $\tilde{g} > 1$ , and (c):  $V_0 = 0.3511$  at the critical point  $\tilde{g} = 1$ . Panel (a) is for the condensate in the exact Bloch state (7), and panel (b) is for the condensate in the exact Bloch state (11). Solutions (7) and (11) are twofold degenerate Bloch states, which coalesce into one single state at the critical point. All figures show that the density peaks situate at the valleys of lattice potential wells. The other parameters are  $g = 0.5, \Omega = 0.3, k_0 = 0.4$ . Plotted quantities are in normalized units.

(11) can be obtained by only interchanging the expressions  $C_1$  and  $C_2$  of Eq. (7). Solutions (7) and (11) are a pair of degenerate Bloch states to Eq. (6) for a quasimomentum corresponding to the boundary of the first Brillouin zone. From a mathematical point of view, these two extra exact Bloch solutions originate from nonlinear bifurcation. This leads to a natural speculation that above a critical nonlinearity, swallowtail (or loop) would develop in the band near the zone boundary for a SO-coupled BEC lattice system, as is the case for the regular BEC in optical lattice. The looped band structure should be

further explored by numerical method.

With the exact solutions, the densities  $n_j = |\psi_j|^2$  of each spin component are given by

$$|\psi_1|^2 = C_1^2 \sin^2 \frac{\theta}{2} + C_2^2 \cos^2 \frac{\theta}{2} + C_1 C_2 \sin \theta \cos(2x), \quad (12)$$

$$|\psi_2|^2 = C_1^2 \cos^2 \frac{\theta}{2} + C_2^2 \sin^2 \frac{\theta}{2} + C_1 C_2 \sin \theta \cos(2x), \quad (13)$$

and the total density takes the form

$$n(x) = |\psi_1|^2 + |\psi_2|^2 = 1 + 2C_1 C_2 \sin \theta \cos(2x), \quad (14)$$

where  $C_1 C_2 = V_0 / (4g \sin \theta)$ .

Equation (14) shows that the contrast in  $n(x)$  is set by  $2C_1 C_2 \sin \theta = V_0 / (2g)$ , independent of the SO coupling strength  $k_0$  and Raman frequency  $\Omega$ . At the critical point  $\tilde{g} = 1$ , we have  $C_1 = C_2 = 1/\sqrt{2}$ , and the two degenerate Bloch states (7) and (11) merge into one single solution with  $|\psi_1|^2 = |\psi_2|^2$ , which is mathematically equivalent to the stripe phase (an equal-weight superposition of two plane wave states) existing in the uniform system[15]. In Fig. 2 we show the density profile calculated at  $g = 0.5, \Omega = 0.3, k_0 = 0.4$ . The two panels (a) and (b) (with  $V_0 = 0.34$ ) correspond to the exact solutions (7) and (11) respectively, and panel (c) corresponds to the exact solution at the critical point  $\tilde{g} = 1$ . When  $\tilde{g} > 1$  is set, as shown in Figs. 2 (a) and (b), the spatial distributions for atomic number densities of two components are parallel, whose amplitude maxima align to the local minima of optical lattice. By comparing Figs. 2 (a) with (b), we readily see that the numbers of atoms in each component for the two exact solutions (7) and (11) are just swapped. At the critical point  $\tilde{g} = 1$ , the two spin components feature the same spatial distribution [see Fig. 2 (c)].

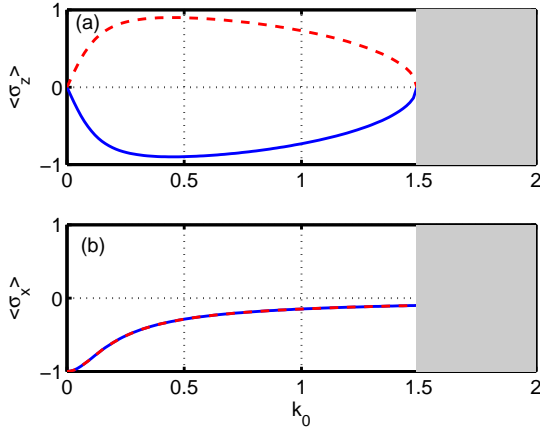


FIG. 3: (color online) Longitudinal and transverse spin polarization  $\langle \sigma_z \rangle$  and  $\langle \sigma_x \rangle$  as a function of SO coupling strength  $k_0$ . The blue lines and red dashed lines denote spin polarizations of exact solutions (7) and (11) respectively, and shaded areas correspond to the regions where these exact solutions (7) and (11) no longer exist. The other parameters are  $g = 0.5, V_0 = 0.1, \Omega = 0.3$ . Plotted quantities are in normalized units.

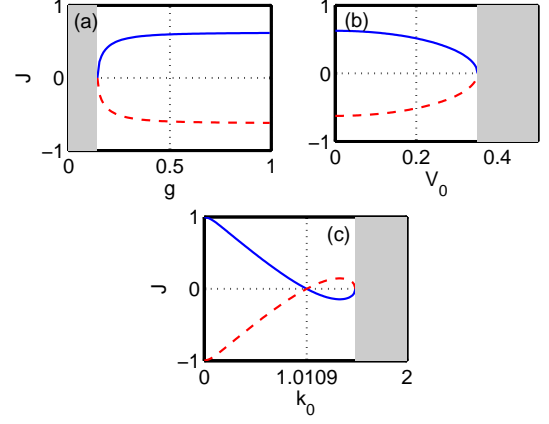


FIG. 4: (color online) (a) The atomic current density  $J$  versus non-linearity value  $g$ . The other parameters are chosen as  $V_0 = 0.1, k_0 = 0.4, \Omega = 0.3$ . (b) The atomic current density  $J$  versus lattice depth  $V_0$ . The other parameters are chosen as  $g = 0.5, k_0 = 0.4, \Omega = 0.3$ . (c) The atomic current density  $J$  versus SO coupling strength  $k_0$ . The other parameters are chosen as  $g = 0.5, V_0 = 0.1, \Omega = 0.3$ . In all plots, the blue lines and red dashed lines describe the current densities of exact solutions (7) and (11) respectively, and shaded areas correspond to the regions where these exact solutions (7) and (11) no longer exist. Plotted quantities are in normalized units.

To put the exact Bloch states into perspective, we further calculate the key physical quantities such as the longitudinal ( $\langle \sigma_z \rangle$ ) and transverse ( $\langle \sigma_x \rangle$ ) spin polarization of the gas

$$\langle \sigma_z \rangle = \frac{1}{\pi} \int_{-\pi/2}^{\pi/2} (|\psi_1|^2 - |\psi_2|^2) dx = \cos \theta (|C_2|^2 - |C_1|^2), \quad (15)$$

$$\langle \sigma_x \rangle = \frac{1}{\pi} \int_{-\pi/2}^{\pi/2} (\psi_1^* \psi_2 + \psi_1 \psi_2^*) dx = -\sin \theta. \quad (16)$$

The longitudinal spin polarizations characterizing the two exact Bloch states (7) and (11) are then given by the simple expression  $\langle \sigma_z \rangle = \pm \cos \theta \sqrt{1 - V_0^2 / (4g^2 \sin^2 \theta)}$  [- for solution (7) and + for solution (11)], while the transverse polarizations are given by the same value  $\langle \sigma_x \rangle = -\sin \theta$ . This implies that the two exact Bloch states (7) and (11) have opposite longitudinal spin polarizations and yet identical transverse polarizations. At the critical point  $\tilde{g} = 1$ , when the condensate is in the single-momentum phase of exact Bloch state with  $C_1 = C_2 = 1/\sqrt{2}$  at the Brillouin zone edge, the longitudinal spin polarization identically vanishes:  $\langle \sigma_z \rangle = 0$ , while  $\langle \sigma_x \rangle \neq 0$ . This unique single-momentum phase has no analog in homogeneous systems, which seems reminiscent of the Bloch state at the edge of the Brillouin zone numerically found in the same SO-coupled BEC lattice system[23].

In Fig. 3, we plot the longitudinal and the transverse spin polarizations  $\langle \sigma_z \rangle$  [Fig. 3(a)] and  $\langle \sigma_x \rangle$  [Fig. 3(b)] as a function of the SO coupling strength  $k_0$ . As shown in Fig. 3, when  $\tilde{g} > 1$  (on the left side of the shaded area), the exact Bloch wave states (7) and (11) with wave vector  $k = 1$  describe the single-momentum phase with both nonzero longitudinal and

transverse spin polarizations. Here, the red dashed lines correspond to the spin polarization of the exact Bloch wave state (7) and the blue solid lines correspond to the spin polarization of the exact Bloch wave state (11). An exceptional point is that at  $k_0 = 0$  (in the absence of SO coupling),  $\langle \sigma_z \rangle$  vanishes, which indicates the longitudinal spin polarization arising from SO coupling. However, as the SO coupling strength  $k_0$  increases to the boundary of the shaded area [that is, the critical point  $\tilde{g} = 1$  is reached], the system enters a new phase characterized by the merged exact Bloch wave state with  $\langle \sigma_z \rangle = 0$  and  $\langle \sigma_x \rangle \neq 0$ .

As is well known, all the linear Bloch waves at the zone edge carry no currents, because the flow  $\exp(ix)$  for free particle is stopped completely by Bragg scattering from the periodic potential. For the regular BEC without SO coupling, when the nonlinearity is strong enough to dominate the competition between the periodic potential and the nonlinear mean-field interaction, the flow can no longer be stopped by Bragg scattering, leading to a current-carrying Bloch wave at the edge. Such a superfluidity is related to the appearance of a loop (also called swallowtail) structure in the energy dispersion. And then a question naturally arises: what new effects will the superflow have in the SO-coupled BEC lattice system?

With the exact solutions at hand, we can directly examine the superfluidity. From the continuity equation,  $(d/dt)n(x) + \nabla \cdot \vec{J} = 0$  (in our case,  $\vec{J} = J\vec{i}$ ), it follows that the atomic current density of the condensate can be written as

$$J = \frac{i}{2} \left( \frac{d\psi^\dagger}{dx} \psi - \psi^\dagger \frac{d\psi}{dx} \right) - k_0 \psi^\dagger \hat{\sigma}_z \psi = (|C_1|^2 - |C_2|^2)(1 - k_0 \cos \theta), \quad (17)$$

where the second part in current density is induced by the SO coupling. Note that Eq. (2) is an effective Hamiltonian that describes SO coupling in the frame transformed via the local pseudospin rotation. To look into the current density (17) in laboratory reference frame, we apply a unitary transformation to the wave functions  $\phi_1 = \psi_1 e^{ik_0 x}$  and  $\phi_2 = \psi_2 e^{-ik_0 x}$ , and the original Hamiltonian in laboratory frame for  $\phi = (\phi_1, \phi_2)^T$  is  $H_{\text{lab}} = \frac{\hat{p}_x^2}{2} + \frac{\Omega}{2}(e^{i2k_0 x} \hat{\sigma}_+ + e^{-i2k_0 x} \hat{\sigma}_-) + V_0 \sin^2(x) + \hat{H}_{\text{non}}$ , where  $\hat{\sigma}_\pm = \hat{\sigma}_x \pm i\hat{\sigma}_y$ . When moving back to the laboratory frame, we can employ the conventional current density  $J = \frac{i}{2} \left( \frac{d\phi^\dagger}{dx} \phi - \phi^\dagger \frac{d\phi}{dx} \right)$  to yield the same formula (17). The result is obvious because all the physical observable quantities are independent of reference frame.

In Fig. 4, we plot the atomic current density  $J$  versus the system parameters such as the nonlinearity value  $g$ , lattice depth  $V_0$ , and SO coupling strength  $k_0$ . As shown in Fig. 4, the two exact solutions (7) and (11) represent the flow of non-zero speed with opposite signs except at the critical point  $\tilde{g} = 1$  (at the boundaries of the shaded areas) as illustrated by the blue lines and red dashed lines respectively. These two exact states share the same crystal momentum  $k = 1$  but have different atomic current velocities, where the solution (7) corresponds to the fluid moving to the right, whereas the other solution (11) corresponds to fluid moving towards the left. The current-carrying Bloch wave states at the Brillouin zone edge are a

manifestation of superfluidity. At the critical point  $\tilde{g} = 1$  [i.e., at the boundaries of the shaded areas], the current densities  $J$  of these two exact states identically disappear. This follows because  $|C_1|^2 = |C_2|^2$  at the critical point. In the absence of SO coupling ( $k_0 = 0$ ), the two exact solutions (7) and (11) carry nonzero total density currents,  $J = \pm \sqrt{4g^2 - V_0^2}/(2g)$ . Another nontrivial finding is that at a particular SO coupling strength  $k_0 = 1.0109$  corresponding to  $k_0 \cos \theta = 1$  [marked by vertical line in Fig. 4(c)], the two atomic current densities vanish due to the competition between nonlinearity and SO coupling. This result occurs uniquely in the SO-coupled BEC lattice system.

Apart from the continuity equation for total atomic density current, there also exists a continuity equation for the spin density and spin current, which is given by[45]

$$\frac{d}{dt} \vec{s}(x, t) = -\nabla \cdot \vec{j}_s(x, t) + \vec{j}_\omega(x, t). \quad (18)$$

In Eq. (18), the spin density  $\vec{s}$  is defined as  $\vec{s}(x, t) = \Psi^\dagger \hat{s} \Psi$  with  $\hat{s} = (1/2)\hat{\sigma}$  and  $\hat{\sigma} = \hat{\sigma}_x \vec{i} + \hat{\sigma}_y \vec{j} + \hat{\sigma}_z \vec{k}$ . The tensor  $\vec{j}_s$  and the vector  $\vec{j}_\omega$  are named the linear and the angular spin current densities respectively[45]. Here we only focus on the quantity  $\vec{j}_s$ , which describes the translational motion of a spin. As for our model, the linear spin current densities take the form

$$\vec{j}_s(x, t) = \text{Re} \left\{ \Psi^\dagger \hat{v} \hat{s} \Psi \right\} = \text{Re} \left\{ \Psi^\dagger [\hat{p}_x \vec{i} + k_0 \hat{\sigma}_z \vec{i}] \hat{s} \Psi \right\}. \quad (19)$$

Thus, the spin current density tensor  $\mathbf{j}_s^\nu$  ( $\nu = x, y, z$  denotes the spin component) is

$$\mathbf{j}_s^\nu(x, t) = \text{Re} \left\{ \Psi^\dagger [\hat{p}_x \vec{i} + k_0 \hat{\sigma}_z \vec{i}] \hat{s}_\nu \Psi \right\}. \quad (20)$$

By taking  $z$ -component of spin as an example, we perform some simple calculations and derive the analytical spin current density  $\mathbf{j}_s^z$  carried by the exact Bloch states (7) and (11),

$$\mathbf{j}_s^z(x, t) = -\frac{\cos \theta}{2} \vec{i} + \frac{k_0}{2} \left[ 1 + \frac{V_0}{2g} - \frac{V_0}{g} \sin^2(x) \right] \vec{i}. \quad (21)$$

From Eq. (21), we know that these exact Bloch states presented here do carry the spin currents. According to Eqs. (17) and (21), when  $k_0 \cos \theta = 1$ , the total density current vanishes, while the spin current is nonzero. It is analytically shown that these exact nonlinear Bloch wave states (7) and (11) carry no total density current and only pure spin current. This gives an exact demonstration of the pure spin current discussed in the literatures (see, for example, Ref. [46]).

So far, our investigations are limited to the case of symmetric spin interaction with all equal nonlinearities  $g_{11} = g_{22} = g_{12}$ . We find that for the case of the intercomponent interaction not equal to the intracomponent interaction, i.e.,  $g_{11} = g_{22} \neq g_{12}$ , when  $g_{11} + g_{12} = V_0/\sin \theta$ , the GP equation (1) also admits exact solution of nonlinear Bloch state at the Brillouin zone edge in the form of  $\psi = \frac{1}{\sqrt{2}} e^{ix} (\sin(\theta/2), -\cos(\theta/2))^T + \frac{1}{\sqrt{2}} e^{-ix} (\cos(\theta/2), -\sin(\theta/2))^T$ . At present, it remains challenging to find the more generic exact solutions of nonlinear Bloch states at the Brillouin zone edge for asymmetric spin interaction, which deserves further investigation in future work.

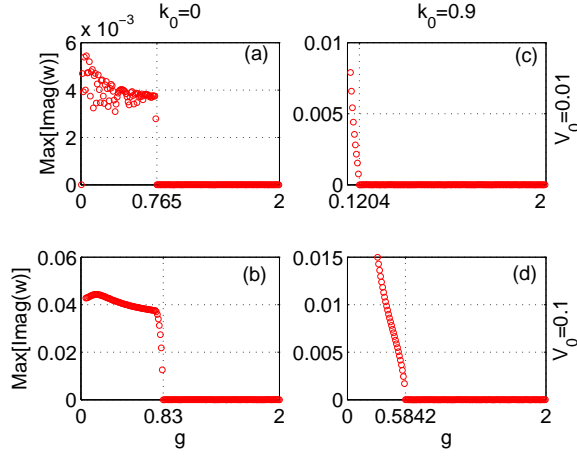


FIG. 5: (color online) Dynamical stability of the exact Bloch solution (7) with crystal momentum  $k = 1$ . Maximum imaginary part of  $w$  versus nonlinearity strength  $g$  for different values of  $k_0$  and  $V_0$ : (a)  $k_0 = 0$ ,  $V_0 = 0.01$ ; (b)  $k_0 = 0$ ,  $V_0 = 0.1$ ; (c)  $k_0 = 0.9$ ,  $V_0 = 0.01$ ; (d)  $k_0 = 0.9$ ,  $V_0 = 0.1$ . Here  $g_{11} = g_{22} = g_{12} = g$  and  $\Omega = 0.3$ . The largest imaginary value of  $w$ ,  $\text{Max}[\text{Imag}(w)]$ , is used to measure the dynamical stability.  $\text{Max}[\text{Imag}(w)] = 0$  indicates dynamical stability and  $\text{Max}[\text{Imag}(w)] \neq 0$  indicates dynamical instability. Plotted quantities are in normalized units.

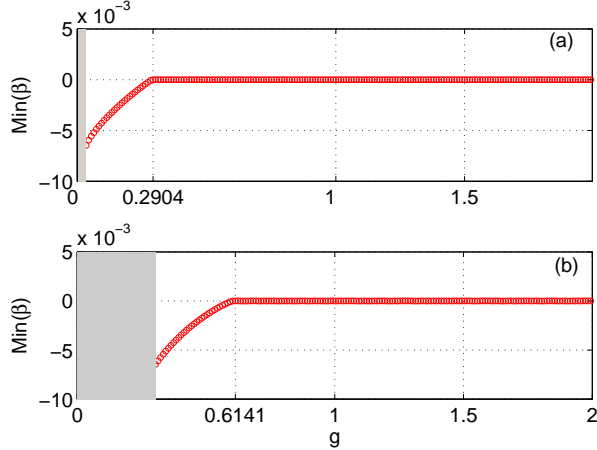


FIG. 6: (color online) Landau stability of the exact Bloch solution (7) with crystal momentum  $k = 1$ . (a) Plot of minimum (i.e., negative maximum) of  $\beta$  versus nonlinearity strength  $g$  with the same system parameters as those in 5 (c). (b) Plot of minimum (i.e., negative maximum) of  $\beta$  versus nonlinearity strength  $g$  with the same system parameters as those in 5 (d). The minimum value of  $\beta$ ,  $\text{Min}(\beta)$ , is used to measure the Landau stability.  $\text{Min}(\beta) = 0$  indicates Landau stability and  $\text{Min}(\beta) < 0$  indicates Landau instability. Shaded areas represent the regions where the exact solution (7) no longer exists. Plotted quantities are in normalized units.

#### IV. STABILITY

Essential to the realizability of these above-mentioned exact Bloch states is their stability. For BEC in optical lattices, there are two ways of destroying superfluidity: dynamical instability and Landau instability (also called energetic instability). Once the exact Bloch states of interest are prepared, their stability can be accurately examined by applying Bogoliubov theory[47]. Assume that the system experiences a small disturbance at a Bloch state:

$$\Psi = e^{-i\mu t} [\psi(x) + \delta\psi(x, t)] = e^{-i\mu t + ikx} [\varphi_k(x) + \delta\varphi(x, t)], \quad (22)$$

where the disturbance can be written as

$$\delta\varphi(x, t) = \begin{pmatrix} U_1(x) \\ U_2(x) \end{pmatrix} \exp(iqx - i\omega t) + \begin{pmatrix} V_1^*(x) \\ V_2^*(x) \end{pmatrix} \exp(-iqx + i\omega^* t), \quad (23)$$

with  $q$  ranging between  $-1$  and  $1$ . Substituting Eqs. (22) and (23) into the time-dependent Gross-Pitaevskii equation (1) and keeping the first-order terms, we obtain the Bogoliubov-Genness (BdG) equation

$$\mathbf{M} \begin{pmatrix} U_1 \\ U_2 \\ V_1 \\ V_2 \end{pmatrix} = w \begin{pmatrix} U_1 \\ U_2 \\ V_1 \\ V_2 \end{pmatrix} \quad (24)$$

with the matrix

$$\mathbf{M} = \begin{pmatrix} \hat{L}_+(k, q) & g_{12}\varphi_2^*\varphi_1 + \frac{\Omega}{2} & g_{11}\varphi_1^2 & g_{12}\varphi_2\varphi_1 \\ g_{12}\varphi_1^*\varphi_2 + \frac{\Omega}{2} & \hat{L}_-(k, q) & g_{12}\varphi_1\varphi_2 & g_{22}\varphi_2^2 \\ -g_{11}\varphi_1^{*2} & -g_{12}\varphi_2^*\varphi_1^* & -\hat{L}_+(k, -q) & -g_{12}\varphi_1^*\varphi_2 - \frac{\Omega}{2} \\ -g_{12}\varphi_1^*\varphi_2^* & -g_{22}\varphi_2^{*2} & -g_{12}\varphi_2^*\varphi_1 - \frac{\Omega}{2} & -\hat{L}_-(k, -q) \end{pmatrix}, \quad (25)$$

and

$$\begin{aligned}\hat{L}_+(k, q) &= -\frac{1}{2} \left[ \frac{\partial}{\partial x} + i(q+k) \right]^2 - ik_0 \left[ \frac{\partial}{\partial x} + i(q+k) \right] + V(x) - \mu \\ &\quad + 2g_{11} |\psi_1|^2 + g_{12} |\psi_2|^2, \\ \hat{L}_-(k, q) &= -\frac{1}{2} \left[ \frac{\partial}{\partial x} + i(q+k) \right]^2 + ik_0 \left[ \frac{\partial}{\partial x} + i(q+k) \right] + V(x) - \mu \\ &\quad + 2g_{22} |\psi_2|^2 + g_{12} |\psi_1|^2.\end{aligned}\quad (26)$$

Note that the matrix  $M$  is not Hermitian and its eigenvalues  $w$  are not necessarily all real. In Eq. (24), if any eigenvalue  $w$  has imaginary part, the nonlinear Bloch wave is dynamically unstable; if otherwise, i.e., eigenvalues  $w$  are real for all  $-1 \leq q < 1$ , it is dynamically stable.

The dynamical stabilities of the exact Bloch solution (7) are numerically computed and shown in Fig. 5 with different values of  $k_0$  and  $V_0$ , where the dynamical stability is measured by the largest imaginary value of the eigenvalues  $w$ . If the maximum of the imaginary part of  $w$  is zero, the solution is dynamically stable; otherwise, certain modes of perturbation grow exponentially with time, and thus the solution is unstable and the superflow breaks down. It is clear from Fig. 5 that the exact Bloch solution (7) is dynamically stable when the atomic interaction  $g$  is beyond certain critical values (marked by vertical lines). The critical values of  $g$ , above which the exact Bloch wave (7) is dynamically stable, decrease with increasing the SO coupling from  $k_0 = 0$  (absence of SO coupling) to  $k_0 = 0.9$  as we see in each row. On the other hand, the critical value of  $g$  for the dynamical stability increases with the lattice potential strength  $V_0$ , as can be seen by comparison of the two rows of Fig. 5.

The onset of Landau instability can be investigated numerically by solving the BdG equation  $\tau_z \mathbf{M} \mathbf{u} = \beta \mathbf{u}$  with  $\tau_z = \hat{\sigma}_z \otimes I$  and  $\mathbf{u} = (U_1, U_2, V_1, V_2)^T$ . If any of eigenvalues  $\beta$  is negative, elementary excitations associated with the perturbations will be energetically preferable, causing Landau instability (superfluidity is lost). In Fig. 5, the minimum (i.e., negative maximum) of  $\beta$  is plotted, where nonzero values indicate the Landau instability and zero values indicate the Landau stability. There also exist critical values of  $g$  beyond which the Bloch wave (7) is Landau stable and it represents a superflow. For comparison, the system parameters in Figs. 6 (a) and (b) are set to be the same as those in Figs. 5 (c) and (d) respectively. By comparison we find that the critical values of  $g$  for dynamical stability are smaller than the counterparts for Landau stability. This means that the exact Bloch wave (7) with dynamical instability must be Landau unstable, whereas the Bloch wave with Landau instability is not necessarily dynamically unstable. These properties are in analogy to the ones of regular BEC lattice system[41]. The same results of stability analysis hold true for the other degenerate Bloch wave (11).

## V. CONCLUSIONS

In conclusion, we have reported simple but generic twofold degenerate exact solutions of current-carrying nonlin-

ear Bloch states at the Brillouin zone edge in the SO-coupled lattice BEC system with a symmetric spin interaction. These exact solutions occur only above a critical nonlinearity and thus have no linear counterparts. They are examined in terms of spin polarizations and the condensates superfluid properties. These two degenerate exact Bloch states are shown to share the same crystal momentum but have different atomic flow velocities, one of which corresponds to the fluid moving to the right and the other to fluid moving to the left. We have also demonstrated that the exact analytical solutions possess some intriguing properties that are absent in the regular BECs without SO coupling loaded into optical lattices. For example, for certain SO coupling strengths, the total density current of the superflow at the Brillouin zone edge is zero, but the spin current is nonzero.

From a mathematical perspective, these extra exact nonlinear Bloch solutions emerge due to bifurcation, which makes the nonlinear Bloch band different from the linear case. It leads to a natural speculation that this SO-coupled BEC lattice system would develop a looplike structure at the edge of the nonlinear Bloch band extensively found in the regular BEC lattice systems. Recently, the emergence of looplike structure has been reported numerically in the nonlinear dispersion relation of the SO-coupled BEC in the uniform space[42]. However, our exact solutions provide, for the first time to our knowledge, an analytical evidence for the looplike Bloch band structure in the SO-coupled BEC lattice system, which will give us an intuitive insight to help us understand the superfluidity and other related properties such as hysteresis, Bloch oscillation and nonlinear Landau-Zener tunneling. For the purpose of application, we have analyzed the collective excitations about these exact nonlinear Bloch states and investigated the superfluidity stability through dynamical and Landau stability analysis.

## Acknowledgments

The work was supported by the National Natural Science Foundation of China (Grants No.11975110, No.11764022, No.11465009, and No.11947082), the Zhejiang Provincial Natural Science Foundation of China (Grant No. LY21A050002 and No. LZ20A040002), the Scientific and Technological Research Fund of Jiangxi Provincial Education Department (Grants No.GJJ180559, No.GJJ180581, No.GJJ180588, No.GJJ190549, and No.GJJ190577), and Open Research Fund Program of the State Key Laboratory of Low-Dimensional Quantum Physics (Grant No. KF201903). Yunrong Luo was supported by the Scientific Research Fund of Hunan Provincial Education Department under Grant No. 18C0027 and the National Natural Science Foundation of China under Grants 11747034.

## Appendix

In Appendix, we will give the detailed derivations of the exact solution to the time-independent GP equation (6) in the

main text.

To proceed, we set the test solution of the time-independent GP equation (6) as

$$\begin{pmatrix} \psi_1 \\ \psi_2 \end{pmatrix} = C_1 \begin{pmatrix} \sin \frac{\theta}{2} \\ -\cos \frac{\theta}{2} \end{pmatrix} e^{ix} + C_2 \begin{pmatrix} \cos \frac{\theta}{2} \\ -\sin \frac{\theta}{2} \end{pmatrix} e^{-ix}, \quad (\text{A.1})$$

where  $C_1, C_2$  and  $\theta$  are undetermined parameters. The superposition coefficients  $C_1 = |C_1|e^{i\alpha_1}$  and  $C_2 = |C_2|e^{i\alpha_2}$  satisfy the normalization constraint  $|C_1|^2 + |C_2|^2 = 1$  [corresponding to the normalization  $(1/\pi) \int_{-\pi/2}^{\pi/2} dx (|\psi_1|^2 + |\psi_2|^2) = 1$ ]. It follows from (A.1) that

$$|\psi_1|^2 = |C_1|^2 \sin^2 \frac{\theta}{2} + |C_2|^2 \cos^2 \frac{\theta}{2} + |C_1||C_2| \sin \theta \cos(2x + \beta), \quad (\text{A.2})$$

$$|\psi_2|^2 = |C_1|^2 \cos^2 \frac{\theta}{2} + |C_2|^2 \sin^2 \frac{\theta}{2} + |C_1||C_2| \sin \theta \cos(2x + \beta), \quad (\text{A.3})$$

where  $\beta = \alpha_1 - \alpha_2$  is the phase of  $C_1 C_2^*$ . Then we have

$$|\psi_1|^2 + |\psi_2|^2 = 1 + 2|C_1||C_2| \sin \theta - 4|C_1||C_2| \sin \theta \sin^2 \left( x + \frac{\beta}{2} \right), \quad (\text{A.4})$$

where  $|C_1|^2 + |C_2|^2 = 1$  has been used. It can be easily verified that under the balanced conditions  $4g|C_1||C_2| \sin \theta = V_0$  and  $\beta = 0$ , the following relation is automatically established

$$g(|\psi_1|^2 + |\psi_2|^2) + V_0 \sin^2(x) = \frac{V_0}{2} + g. \quad (\text{A.5})$$

The requirements of the two equations  $4g|C_1||C_2| \sin \theta = V_0$  and  $|C_1|^2 + |C_2|^2 = 1$  yield

$$|C_1|^2 = \frac{1}{2} \pm \frac{1}{2} \sqrt{1 - \frac{V_0^2}{4g^2 \sin^2 \theta}}, \quad (\text{A.6})$$

$$|C_2|^2 = \frac{1}{2} \mp \frac{1}{2} \sqrt{1 - \frac{V_0^2}{4g^2 \sin^2 \theta}}. \quad (\text{A.7})$$

As long as the modulus of coefficients  $C_1$  and  $C_2$  is fixed by the above two equations (A.6) and (A.7), and the relative

phase between the coefficients  $C_1$  and  $C_2$  is by  $\beta = 0$ , Eq. (6) in the main text is reduced to the linear Schrödinger equation

$$\left[ \hat{H}_{\text{soc}} + \frac{V_0}{2} + g \right] \psi = \mu \psi. \quad (\text{A.8})$$

The parameter  $\theta$  in the ansatz (A.1) can be determined by the above linear Schrödinger equation (A.8). If the parameter  $\theta$  matches the following relationship

$$\sin \theta = \frac{\Omega}{2\sqrt{\frac{\Omega^2}{4} + k_0^2}}, \quad \cos \theta = \frac{k_0}{\sqrt{\frac{\Omega^2}{4} + k_0^2}}, \quad (\text{A.9})$$

the ansatz (A.1) is just the exact solution of Eq. (A.8). In fact, under condition (A.9), the wave functions  $e^{ix}(\sin(\theta/2), -\cos(\theta/2))^T$  and  $e^{-ix}(\cos(\theta/2), -\sin(\theta/2))^T$  are two-fold degenerate eigenstates of the linear Schrödinger equation (A.8). Therefore, the linear combination of two degenerate eigenstates is also an eigenstate of equation (A.8) with the same eigenvalue.

Given Eqs. (A.6)-(A.7) and Eq. (A.9), together with  $\beta = 0$ , Eq. (A.1) constitutes two degenerate exact Bloch solutions to Eq. (6) at the Brillouin zone edge  $k = 1$ . From Eqs. (A.6)-(A.7), we can readily observe that the superposition coefficients  $C_1$  and  $C_2$  are given by (up to a trivial global phase  $\alpha_1 = \alpha_2$ )

$$\begin{aligned} C_1 = |C_1| &= \left( \frac{1}{2} \pm \frac{1}{2} \sqrt{1 - \frac{V_0^2}{4g^2 \sin^2 \theta}} \right)^{1/2} \\ &= \frac{\sqrt{g + \frac{V_0}{2 \sin \theta}} \pm \sqrt{g - \frac{V_0}{2 \sin \theta}}}{2\sqrt{g}}, \end{aligned} \quad (\text{A.10})$$

$$\begin{aligned} C_2 = |C_2| &= \left( \frac{1}{2} \mp \frac{1}{2} \sqrt{1 - \frac{V_0^2}{4g^2 \sin^2 \theta}} \right)^{1/2} \\ &= \frac{\sqrt{g + \frac{V_0}{2 \sin \theta}} \mp \sqrt{g - \frac{V_0}{2 \sin \theta}}}{2\sqrt{g}}, \end{aligned} \quad (\text{A.11})$$

which exactly correspond to the two exact solutions (7) and (11) in the main text.

---

[1] X. L. Qi and S. C. Zhang, *Physics Today* **63**, 33 (2010); M. Z. Hasan and C. L. Kane, *Rev. Mod. Phys.* **82**, 3045 (2010).  
[2] Y. K. Kato, R. C. Myers, A. C. Gossard, and D. D. Awschalom, *Science* **306**, 1910 (2004).  
[3] I. Žutić, J. Fabian, and S. Das Sarma, *Rev. Mod. Phys.* **76**, 323 (2004); J. D. Koralek, C. P. Weber, J. Orenstein, B. A. Bernevig, S. C. Zhang, S. Mack, and D. D. Awschalom, *Nature (London)* **458**, 610 (2009);  
[4] Y. J. Lin, K. Jiménez-García, and I. B. Spielman, *Nature (London)* **471**, 83 (2011).  
[5] P. J. Wang, Z. Q. Yu, Z. K. Fu, J. Miao, L. H. Huang, S. J. Chai, H. Zhai, and J. Zhang, *Phys. Rev. Lett.* **109**, 095301 (2012).

[6] L. W. Cheuk, A. T. Sommer, Z. Hadzibabic, T. Yefsah, W. S. Bakr, and M. W. Zwierlein, *Phys. Rev. Lett.* **109**, 095302 (2012).  
[7] J. Zhang, S. Ji, Z. Chen, L. Zhang, Z. Du, B. Yan, G. Pan, B. Zhao, Y. Deng, H. Zhai, S. Chen, and J. Pan, *Phys. Rev. Lett.* **109**, 115301 (2012).  
[8] L. Huang, Z. Meng, P. Wang, P. Peng, S. L. Zhang, L. Chen, D. Li, Q. Zhou, and J. Zhang, *Nat. Phys.* **12**, 540 (2016).  
[9] Z. Wu, L. Zhang, W. Sun, X. T. Xu, B. Z. Wang, S. C. Ji, Y. Deng, S. Chen, X. J. Liu, and J. W. Pan, *Science* **354**, 83 (2016).  
[10] C. Wang, C. Gao, C.-M. Jian, and H. Zhai, *Phys. Rev. Lett.* **105**, 160403 (2010).



- [11] T.-L. Ho and S. Zhang, *Phys. Rev. Lett.* 107, 150403 (2011).
- [12] C.-J. Wu, I. Mondragon-Shem, and X.-F. Zhou, *Chin. Phys. Lett.* 28, 097102 (2011).
- [13] M. A. Khamehchi, Y. Zhang, C. Hamner, T. Busch, and P. Engels, *Phys. Rev. A* 90, 063624 (2014).
- [14] S.-C. Ji, L. Zhang, X.-T. Xu, Z. Wu, Y. Deng, S. Chen, and J.-W. Pan, *Phys. Rev. Lett.* 114, 105301 (2015).
- [15] Y. Li, L. P. Pitaevskii, and S. Stringari, *Phys. Rev. Lett.* 108, 225301 (2012).
- [16] Z. Cai, X. Zhou, and C. Wu, *Phys. Rev. A* 85, 061605(R) (2012).
- [17] W. S. Cole, S. Zhang, A. Paramekanti, and N. Trivedi, *Phys. Rev. Lett.* 109, 085302 (2012).
- [18] J. Radić, A. Di Ciolo, K. Sun, and V. Galitski, *Phys. Rev. Lett.* 109, 085303 (2012).
- [19] Y. V. Kartashov, V. V. Konotop, D. A. Zezyulin, and L. Torner, *Phys. Rev. Lett.* 117, 215301 (2016).
- [20] Y. Zhang and C. Zhang, *Phys. Rev. A* 87, 023611 (2013).
- [21] L. Zhou, H. Pu, and W. Zhang, *Phys. Rev. A* 87, 023625 (2013).
- [22] C. Hamner, Y. Zhang, M. A. Khamehchi, M. J. Davis, and P. Engels, *Phys. Rev. Lett.* 114, 070401 (2015).
- [23] Z. Chen and Z. Liang, *Phys. Rev. A* 93(1), 013601 (2016).
- [24] B. T. Seaman, L. D. Carr, and M. J. Holland, *Phys. Rev. A* 71, 033622 (2005).
- [25] W. D. Li and A. Smerzi, *Phys. Rev. E* 70, 016605 (2004).
- [26] J. C. Bronski, L. D. Carr, B. Deconinck, and J. N. Kutz, *Phys. Rev. Lett.* 86, 1402 (2001).
- [27] J. C. Bronski, L. D. Carr, B. Deconinck, J. N. Kutz, and K. Promislow, *Phys. Rev. E* 63, 036612 (2001).
- [28] J. C. Bronski, L. D. Carr, R. Carretero-González, B. Deconinck, J. N. Kutz, and K. Promislow, *Phys. Rev. E* 64, 056615 (2001).
- [29] B. Deconinck, B. A. Frigyyik, and J. N. Kutz, *Phys. Lett. A* 283, 177 (2001).
- [30] N. A. Kostov, V. Z. Enolskii, V. S. Gerdjikov, V. V. Konotop, and M. Salerno, *Phys. Rev. E* 70, 056617 (2004).
- [31] W. Hai, Y. Li, B. Xia, and X. Luo, *Europhys. Lett.*, 71, 28 (2005).
- [32] B. Wu, R. B. Diener, and Q. Niu, *Phys. Rev. A* 65, 025601 (2002).
- [33] D. Diakonov, L. M. Jensen, C. J. Pethick, and H. Smith, *Phys. Rev. A* 66, 013604 (2002).
- [34] E. J. Mueller, *Phys. Rev. A* 66, 063603 (2002).
- [35] M. Machholm, C. J. Pethick, and H. Smith, *Phys. Rev. A* 67, 053613 (2003).
- [36] B. T. Seaman, L. D. Carr, and M. J. Holland, *Phys. Rev. A* 72, 033602 (2005).
- [37] G. Watanabe, S. Yoon, and F. Dalfovo, *Phys. Rev. Lett.* 107, 270404 (2011).
- [38] H. Y. Hui, R. Barnett, J. V. Porto, and S. Das Sarma, *Phys. Rev. A* 86, 063636 (2012).
- [39] D. Yu, W. Yi, and W. Zhang, *Phys. Rev. A* 92, 033623 (2015).
- [40] S. B. Koller, E. A. Goldschmidt, R. C. Brown, R. Wyllie, R. M. Wilson, and J. V. Porto, *Phys. Rev. A* 94, 063634 (2016).
- [41] B. Wu and Q. Niu, *New J. Phys.* 5, 104 (2003).
- [42] Y. Zhang, Z. Gui, and Y. Chen, *Phys. Rev. A* 99, 023616 (2019).
- [43] Y. Wei, C. Kong, and W. Hai, *Chin. Phys. B* 28, 056701 (2019).
- [44] J.-R. Li, J. Lee, W. Huang, S. Burchesky, B. Shteynas, F. Ç. Top, A. O. Jamison, and W. Ketterle, *Nature (London)* 543, 91 (2017).
- [45] Q.-F. Sun and X. C. Xie, *Phys. Rev. B* 72, 245305 (2005).
- [46] Q. Zhu, Q.-F. Sun, and B. Wu, *Phys. Rev. A* 91, 023633 (2015).
- [47] B. Wu and Q. Niu, *Phys. Rev. A* 64, 061603(R) (2001).